To appear in 2009 AIAA GNC, *Invited session on UAV Cooperative Control Technologies for Integrated Defense*

Coordinated Perimeter Patrol with Minimum-Time Alert Response

Derek A. Paley*
University of Maryland, College Park, Maryland, 20742, USA
Laszlo Techy† and Craig A. Woolsey‡
Virginia Polytechnic Institute and State University, Blacksburg, VA, 24061, USA

This paper describes a decentralized feedback framework for coordinated base defense with multiple UAVs. Each UAV is modeled as a constant-speed particle moving in a plane, equipped with steering control and a downward-looking intruder sensor. The feedback framework enables a UAV team flying in a steady, uniform wind to (1) cooperatively patrol a convex perimeter and (2) optimally prosecute intruder alerts. The coordination of patrolling UAVs minimizes coverage gaps in space and time. Each intruder alert is prosecuted by a nearby UAV on a time-optimal path that minimizes response time. After passing over an alert site, the prosecuting UAV resumes the coordinated patrol. This algorithm provides continuous monitoring of a base perimeter and prompt response to intruder alerts with minimal human intervention.

Nomenclature

r_k	Position of kth UAV
$\dot{r}_k$	Inertial velocity of kth UAV
C	Convex loop that circumscribes the base perimeter
c_k	Center of loop traversed by kth UAV
κ_k	Curvature of C at r_k
θ_k	Orientation of velocity of particle k relative to wind direction
γ_k	Orientation of inertial velocity of particle k
ψ_k	Time-phase of particle k on C

Subscript

k, j	Particle indices

I. Introduction

This paper describes a decentralized feedback framework for coordinated control of multiple UAVs in base defense. Each UAV is modeled as a constant speed particle moving in a plane, equipped with steering control and a downward-looking intruder sensor. The feedback framework enables a UAV team flying in a steady, uniform wind to (1) cooperatively patrol a convex perimeter and (2) optimally prosecute intruder alerts. The coordination of patrolling UAVs minimizes coverage gaps in space and time. Each intruder alert is prosecuted by a proximal UAV on a time-optimal path that minimizes response time. After passing over an alert site, the prosecuting UAV resumes the coordinated patrol. This algorithm provides continuous monitoring of a base perimeter and is robust to false alarms and decoys.

*Assistant Professor, Department of Aerospace Engineering, dpaley@umd.edu, AIAA Senior Member.
†Graduate student, Department of Aerospace and Ocean Engineering, techy@vt.edu, AIAA Student Member.
‡Associate Professor, Department of Aerospace and Ocean Engineering, cwoolsey@vt.edu, AIAA Senior Member.

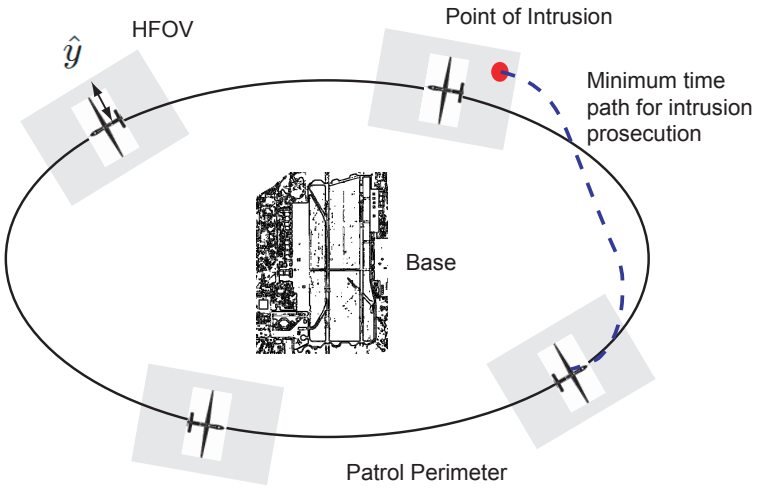

Figure 1. Conceptual sketch of the time-optimal alert response scenario.

The proposed framework for base defense builds on a rigorous mathematical foundation for feedback control of autonomous vehicles modeled as planar, self-propelled particles.[1–3] Cooperative steering algorithms exist to stabilize relative equilibria of the flow-free particle model,[4,5] including parallel and circular formations, as well as formations moving around convex loops.[6] These algorithms employ models of coupled phase oscillators to regulate the spatial separation between particles in simple formations. Recently, steering algorithms have been provided to stabilize collective motion in a time-invariant flowfield,[7] including an algorithm to isolate a time-splay formation—a circular formation in which the particles are uniformly spaced in time.

In this paper, we apply the particle-control approach to the base-defense application. A feedback algorithm is provided to stabilize a time-splay formation in steady, uniform wind on a strictly convex loop that circumscribes the base perimeter. A multi-UAV patrol in a time-splay formation minimizes the spatiotemporal gaps in the perimeter coverage. Consequently, each point on the perimeter is inspected with the maximum frequency permitted by the number of UAVs and length of the perimeter. Analysis of the coverage properties of the time-splay formation is performed using a novel space-time projection.

Prompt response to intruder alerts is achieved via time-optimal path planning in wind. Whenever an alert is generated by a patrolling UAV, the alert is prosecuted by the next UAV in line. The UAV that generates the alert continues on the perimeter patrol; the prosecuting UAV follows a shortcut that minimizes the response time. Minimum-time paths for a Dubin's vehicle in steady wind can be generated using a simple geometric method.[8] Time-optimal path planning in wind has been previously paired with feedback coordination on convex loops in the context of an aerobiological-sampling mission.[9] In the aerobiological-sampling mission, two UAVs coordinate their motion along semicircular trajectories designed to measure the flux of airborne particles. In the base-defense application, an arbitrary number of UAVs can be coordinated.

The paper is organized as follows. Section II introduces the base-defense algorithm. Section III summarizes the mathematical model of the planar dynamics of a UAV team in wind. Section IV describes a decentralized algorithm to stabilize a time-splay formation on a convex loop and reviews a geometric method to generate a time-optimal path for an individual UAV. Simulation results are presented in Section V.

II. Base-Defense Algorithm

Consider a convex perimeter circumscribing a base that must be defended by a collection of N UAVs. We seek an optimal method for patrolling the perimeter *and* responding to intruder alerts along the perimeter, as summarized by the following two objectives:

- In nominal conditions, the UAVs coordinate their motion along the perimeter such that the visitation rate at any given point along the curve is constant.
- If an intruder is detected, one UAV responds in minimum time, while the remaining $N-1$ UAVs continue to patrol the original perimeter.

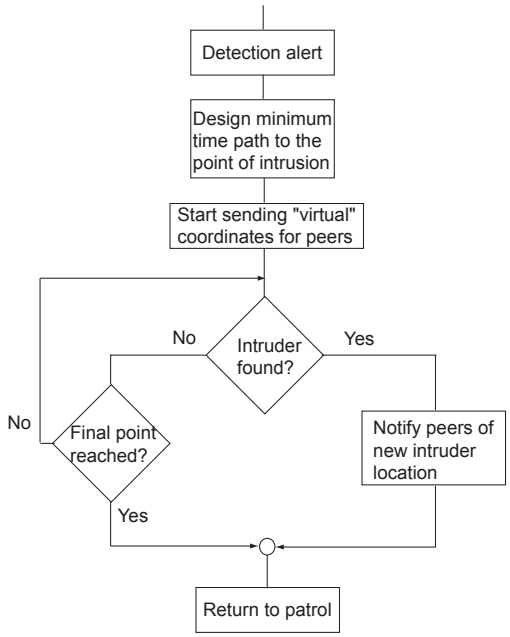

Figure 2. Flow diagram of the time-optimal alert response scenario.

When a threat is detected, there is a trade-off between these two objectives. In one limiting case, the UAVs don't take any action other than reporting the threat and continuing their original, coordinated flight plan. In this case, only the perimeter-patrol objective is achieved. Alternatively, one of the UAVs (e.g., the one that detected the threat) might divert from the perimeter and loiter above the threat. In this case, the number of vehicles covering the perimeter decreases to $N-1$ and gaps in the perimeter coverage increases. Also, if there are N or more simultaneous threats, no UAVs will remain to execute the perimeter-patrol task.

We propose an approach to perimeter surveillance that simultaneously achieves the two goals. Consider the event in which a threat is detected by one of the UAVs (UAV_1) at point r_f; see Figure 1. The alert is reported to the rest of the group, and UAV_1 continues its flight path without diverting to investigate further. The next UAV in sequence (UAV_2) designs a minimum-time flight path from its current location to r_f, and diverts from its original path to reach the threat as quickly as possible.[a]

To ensure that the diversion of UAV_2 does not disrupt the remaining formation (and its perimeter surveillance task), the remaining $N-1$ UAVs assume that UAV_2 is continuing to maintain synchrony, using a *virtual-particle* representation in the coordination algorithm. Once the threat is detected again (or the endpoint of the time-optimal trajectory is reached, whichever occurs first), UAV_2 returns to the original flight plan. If UAV_2 confirms the threat, the next UAV in sequence (UAV_3) is tasked to arrive at the intrusion point in minimum time, and this cycle repeats. A flow-diagram of this can be seen in Figure 2. This approach ensures that the overall perimeter surveillance is not comprised after an individual alert, but it may be susceptible to intruder maneuvering during the handoff between UAV_2 and UAV_3.

Space-time analysis of the base-defense algorithm illustrates how it minimizes the gaps in perimeter coverage. Figure 3(a) depicts the spatiotemporal coverage of a convex perimeter achieved by a single UAV in wind. The UAV trajectory is blue; its sensor swath is gray. Since the perimeter is a closed loop, we identify the left and right edges of the space-time plot. Figure 3(b) depicts the spatiotemporal coverage of a convex perimeter achieved by three coordinated UAVs in wind. The coverage gaps are minimized by a time-splay formation. Figure 3(c) depicts the minimum-time response of a three-UAV patrol to a single intruder alert. The minimum-time shortcut appears as a "hop" rightward and upward on the space-time projection. Subsequent to prosecuting the alert, the UAVs return to a time-splay formation.

[a]Here, we assume the threat is static, or slowly moving, relative to the intercept time for UAV_2. In an interesting variation, one might incorporate an estimate by UAV_1 of the threat's trajectory and modify the intercept path accordingly.

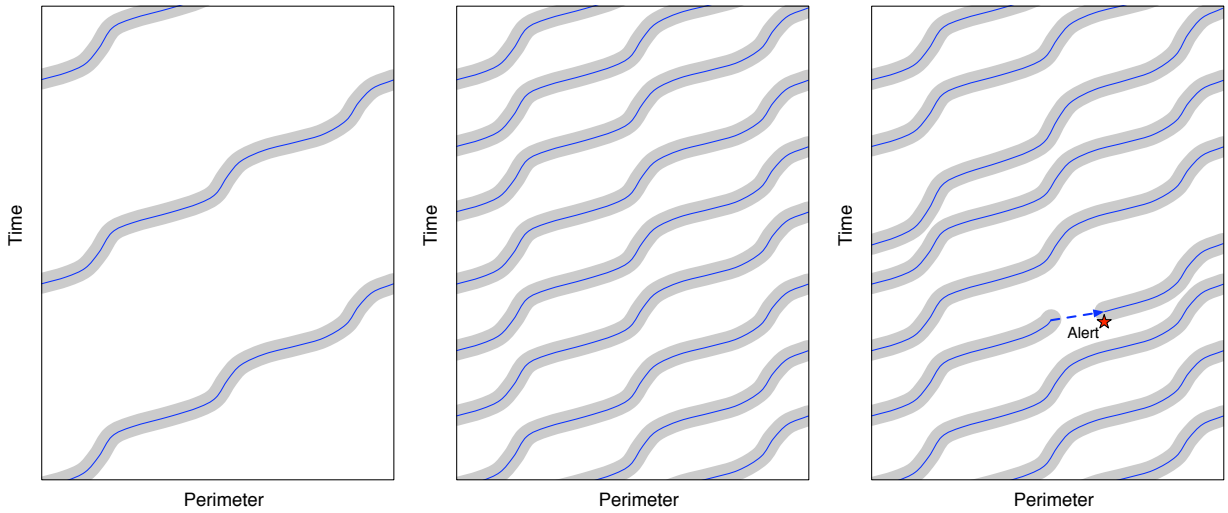

(a) Single UAV Patrol (b) Time-Splay Patrol (Three UAVs) (c) Alert Response

Figure 3. Space-time analysis of coordinated perimeter coverage with time-optimal alert response.

III. UAV Dynamic Model

We represent each UAV as a constant-speed particle moving in a plane subject to steering control and a time-invariant flowfield. The equations of motion of particle $k \in \{1, \ldots, N\}$ in a time-invariant flowfield $f_k = f(r_k)$ are[7]

$$\begin{aligned} \dot{r}_k &= s_0 e^{i\theta_k} + f_k \\ \dot{\theta}_k &= u_k, \end{aligned} \tag{1}$$

where $s_0 e^{i\theta_k}$ is the velocity of k relative to the flow and u_k is the steering control. Let $\dot{r}_k = s_k e^{i\gamma_k}$ represent the velocity of k relative to the ground, where $s_k = |s_0 e^{i\theta_k} + f_k|$ and $\gamma_k = \arg(s_0 e^{i\theta_k} + f_k)$. We have

$$\begin{aligned} \dot{r}_k &= s_k e^{i\gamma_k} \\ \dot{\gamma}_k &= \nu_k, \end{aligned} \tag{2}$$

where $s_k > 0$ and $\nu_k = \nu(u_k)$ is invertible as long as $|f_k| < s_0$ for all r_k. For example, the speed of a unit-speed particle in a steady, uniform flow, $f_k = \beta$, is

$$s_k = \beta \cos \gamma_k + \sqrt{s_0^2 - \beta^2 \sin^2 \gamma_k}. \tag{3}$$

Note, if $\nu_k = \omega_0 s_k$, where $\omega_0 \neq 0$, then particle k orbits a *circle* with radius ω_0^{-1} and fixed center[7]

$$c_k = r_k + \omega_0^{-1} i e^{i\gamma_k}, \tag{4}$$

since, along solutions of (2),

$$\dot{c}_k = (s_k - \omega_0^{-1} \nu_k) e^{i\gamma_k} \equiv 0. \tag{5}$$

IV. Theoretical Results

This section describes a decentralized algorithm to stabilize a time-splay formation on a convex, closed perimeter in a uniform, steady wind. A multi-UAV patrol in a time-splay formation minimizes the spatiotemporal gaps in the perimeter coverage. This section also reviews a geometric method to generate a time-optimal path for an individual UAV to prosecute an alert in minimum time.

IV.A. Coordinated Perimeter Patrol

Let C be a strictly convex loop that circumscribes the base perimeter. If $\nu_k = \kappa_k s_k$, where $\kappa_k = \kappa(\gamma_k)$ is the curvature of C then particle k orbits C and the center c_k of C is fixed.[9] Let $\rho_k = \rho(\phi(\gamma_k)) = r_k - c_k$, where $\rho : \phi \mapsto \rho(\phi)$ and $\phi : \gamma_k \mapsto \phi(\gamma_k)$ are smooth maps. If the inertial velocity of particle k is tangent to C, then

$$e^{i\gamma_k} = \left|\frac{d\rho}{d\phi}\right|^{-1} \frac{d\rho}{d\phi}. \tag{6}$$

and

$$\kappa(\gamma_k) = \frac{d\gamma_k}{d\sigma}, \tag{7}$$

where

$$\sigma(\phi) = \int_0^{\phi} \left|\frac{d\rho}{d\bar{\phi}}\right| d\bar{\phi} \tag{8}$$

is arc length on C. Using (6)–(8), we find

$$\kappa_k^{-1} = \frac{d\sigma}{d\gamma_k} = \frac{d\sigma}{d\phi}\frac{d\phi}{d\gamma_k} = \left|\frac{d\rho}{d\phi}\right| \frac{d\phi}{d\gamma_k}, \tag{9}$$

and

$$\frac{d\rho}{d\gamma_k} = \frac{d\rho}{d\phi}\frac{d\phi}{d\gamma_k} = e^{i\gamma_k}\kappa_k^{-1}. \tag{10}$$

Therefore, along solutions of (2) with $\nu_k = \kappa_k s_k$, we have

$$\dot{c}_k = \dot{r}_k - \frac{d\rho}{d\gamma_k}\dot{\gamma}_k = (s_k - \kappa_k^{-1}\nu_k)e^{i\gamma_k} \equiv 0. \tag{11}$$

Integrating the closed-loop phase dynamics

$$\dot{\gamma}_k = \kappa_k s_k \tag{12}$$

yields

$$t = \int_0^{\gamma_k} \frac{d\gamma}{\kappa(\gamma)s(\gamma)}. \tag{13}$$

The *time-phase*[10] is defined as

$$\psi_k = \psi(\gamma_k) = \frac{2\pi}{T}\int_0^{\gamma_k} \frac{d\gamma}{\kappa(\gamma)s(\gamma)}, \tag{14}$$

where $T > 0$ is the period of a single revolution,

$$T = \int_0^{2\pi} \frac{d\gamma}{\kappa(\gamma)s(\gamma)}. \tag{15}$$

The time-phase (14) represents the progress of particle k around C. Along solutions of (2) we have

$$\dot{\psi}_k = \frac{2\pi}{T}(\kappa_k s_k)^{-1}\nu_k. \tag{16}$$

Equation (16) shows that for the control $\nu_k = \kappa_k s_k$, we have $\dot{\psi}_k = 2\pi/T$, which is constant.

We synthesize a decentralized control that stabilizes a time-splay formation using a Lyapunov-based design. Consider the composite potential[9]

$$V(\boldsymbol{r}, \boldsymbol{\gamma}) = S(\boldsymbol{r}, \boldsymbol{\gamma}) + \frac{T}{2\pi}U(\boldsymbol{\psi}), \tag{17}$$

where $S(\boldsymbol{r}, \boldsymbol{\gamma}) = (1/2)\langle \boldsymbol{c}, P\boldsymbol{c}\rangle$, $P = \mathrm{diag}\{\mathbf{1}\} - \frac{1}{N}\mathbf{1}\mathbf{1}^T$, and $U(\boldsymbol{\psi})$ is a rotationally symmetric phase potential. Since P projects an element of $\mathbb{C}^N$ into the subspace complementary to the span of $\mathbf{1}$, then $S = 0$ if and

only if $c_k = c_j$ for all pairs k, j. Rotational symmetry of U implies $\sum_{j=1}^{N} \frac{\partial U}{\partial \psi_j} = 0$. Along solutions of (2) we have

$$\begin{aligned} \dot{V} &= \sum_{j=1}^{N} \langle e^{i\gamma_j}, P_j \boldsymbol{c} \rangle (s_j - \kappa_j^{-1} \nu_j) + \frac{T}{2\pi} \frac{\partial U}{\partial \psi_j} \dot{\psi}_j \\ &= \sum_{j=1}^{N} \left(s_j \langle e^{i\gamma_j}, P_j \boldsymbol{c} \rangle - \frac{\partial U}{\partial \psi_j} \right) \left(1 - (\kappa_j s_j)^{-1} \nu_j \right), \end{aligned} \tag{18}$$

where P_k is the kth row of L. Choosing the control law

$$\nu_k = \kappa_k s_k \left(1 + K \left(s_j \langle e^{i\gamma_k}, P_k \boldsymbol{c} \rangle - \frac{\partial U}{\partial \psi_k} \right) \right), \; K > 0, \tag{19}$$

enforces convergence of all particles to C with a phase arrangement in the critical set of U. We stabilize a time-splay formation on C by choosing U to be an (M, N)-pattern potential, where $M = N$.[4] The time-splay potential is

$$U^{M,N}(\boldsymbol{\psi}) = \sum_{m=1}^{M} K_m U_m \tag{20}$$

with $K_m > 0$ for $m = 1, \ldots, M-1$ and $K_M < 0$, where

$$U_m(\boldsymbol{\psi}) = \frac{N}{2} |p_{m\psi}|^2, \; p_{m\psi} \triangleq \frac{1}{mN} \sum_{j=1}^{N} e^{im\psi_j}. \tag{21}$$

IV.B. Minimum-Time Alert Response

Consider the initial point $r_0 = x_0 + iy_0$ on the curve C and the final point $r_f = x_f + iy_f$ at the intruder location. The objective is to find minimum time trajectories between the two oriented points. The initial heading angle θ_0 is given and is defined by the curve. The final heading angle can be specified, for simplicity we define it such that the course angle at the intruder location is parallel to the angle of curve C at the projection point. Finding optimal trajectories between initial and final states has been addressed previously,[11] where analytical solutions are presented for a subset of all candidate extremal paths: those for which an initial turn is followed by a straight segment, which is then followed by a second turn in the same direction as the first. The rest of the candidate extremals may be found using a simple numerical root-finding technique.

The paths for which analytical solutions exist form a particularly important subset of all candidate extremals: the curvature along these paths does not change sign. Given a set of waypoints that bound a given closed region in the plane, it is possible to design the connecting paths between these waypoints, such that the resulting closed curve is convex. This property will be exploited to design the patrol perimeter in Section V.B. In what follows, we summarize the path planning method, restricting our attention to the analytical solutions only.[11]

By Pontryagin's minimum principle, the optimal trajectories may contain maximum rate turns and straight segments only.[12,13] Observing that maximum turn rate turns correspond to trochoidal paths,[14] we can search the solutions in terms of path parameter values, where the trochoidal segments and straight lines can be smoothly joined together.[8] Define two trochoidal segments at the initial and final points and a straight segment between the two:[8]

$$x_{t_1}(t) = \frac{s_0}{\delta_1 \omega} \sin(\delta_1 \omega t + \phi_{t_1}) + \beta t + x_{t_{10}} \tag{22}$$

$$y_{t_1}(t) = \frac{-s_0}{\delta_1 \omega} \cos(\delta_1 \omega t + \phi_{t_1}) + y_{t_{10}} \tag{23}$$

$$x_{t_2}(t) = \frac{s_0}{\delta_2 \omega} \sin(\delta_2 \omega t + \phi_{t_2}) + \beta t + x_{t_{20}} \tag{24}$$

$$y_{t_2}(t) = \frac{-s_0}{\delta_2 \omega} \cos(\delta_2 \omega t + \phi_{t_2}) + y_{t_{20}}. \tag{25}$$

Here ω denotes the maximum rate of turn that UAVs are allowed to fly with. The constants $\delta_i \in \{-1, 1\}$ depend on the direction of the turn. Consider the problem of finding the connecting straight path between two trochoidal segments. The connecting line leaves the first trochoid $[x_{t_1}(t), y_{t_1}(t)]^T$ at point A and arrives at the second trochoidal segment $[x_{t_2}(t), y_{t_2}(t)]^T$ at point B. The corresponding path parameter values will be denoted as t_A and t_B. Let $t_{2\pi} = 2\pi/\omega$ denote the time required for the air-relative velocity vector to describe a full circle at the maximum turn rate. We pick the phase angle ϕ_{t_1} and ϕ_{t_2} such that

$$\phi_{t_1} = \theta_0 - \theta_w, \qquad \phi_{t_2} = \theta_f - \theta_w - \delta_2 \omega t_{2\pi},$$

i.e., the first trochoid has the desired initial heading θ_0 at $t = 0$, and the second trochoid has the desired final heading θ_f at $t = t_{2\pi}$. Here θ_w denotes the direction of motion of the ambient air in the inertial frame. Similarly we can pick the constants

$$\begin{aligned} x_{t_{10}} &= x_0 - s_0/(\delta_1\omega)\sin(\phi_{t_1}) \\ y_{t_{10}} &= y_0 + s_0/(\delta_1\omega)\cos(\phi_{t_1}) \\ x_{t_{20}} &= x_f - s_0/(\delta_2\omega)\sin(\delta_2\omega t_{2\pi} + \phi_{t_2}) - \beta t_{2\pi} \\ y_{t_{20}} &= y_f + s_0/(\delta_2\omega)\cos(\delta_2\omega t_{2\pi} + \phi_{t_2}), \end{aligned}$$

such that the first trochoid satisfies the initial conditions $[x_{t_1}(t), y_{t_1}(t)]^T\big|_{t=0} = [x_0, y_0]^T$, and the second trochoid satisfies the final condition $[x_{t_2}(t), y_{t_2}(t)]^T\big|_{t=t_{2\pi}} = [x_f, y_f]^T$. Note that here we assume that the initial and final conditions are already expressed in the trochoidal frame.

With this definition of the constants, we are looking for $t_A \in [0, 2t_{2\pi})$, $t_B \in (-t_{2\pi}, t_{2\pi}]$. The conditions that need to be satisfied can be summarized as follows

- The velocities at point A and point B must be equal:

$$(\dot{x}_{t_1}(t_A), \quad \dot{y}_{t_1}(t_A))^T = (\dot{x}_{t_2}(t_B), \quad \dot{y}_{t_2}(t_B))^T. \tag{26}$$

- The line segment joining the points A and B must be tangent with the velocity vectors at both points:

$$\tan(\alpha) = \frac{y_{t_2}(t_B) - y_{t_1}(t_A)}{x_{t_2}(t_B) - x_{t_1}(t_A)} = \frac{\dot{y}_{t_2}(t_B)}{\dot{x}_{t_2}(t_B)} = \frac{\dot{y}_{t_1}(t_A)}{\dot{x}_{t_1}(t_A)}. \tag{27}$$

- The path parameters must satisfy

$$t_A \in [0, 2t_{2\pi}), \quad t_B \in (-t_{2\pi}, t_{2\pi}]. \tag{28}$$

Condition (26) is equivalent to the condition

$$\delta_1\omega t_A + \phi_{t_1} = \delta_2\omega t_B + \phi_{t_2} + 2k\pi, \qquad k \in \mathbb{Z},$$

where $\mathbb{Z}$ is the set of real integers, and we can express t_B as a function of t_A:

$$t_B = \frac{\delta_1}{\delta_2} t_A + \frac{\phi_{t_1} - \phi_{t_2} + 2k\pi}{\delta_2\omega}, \qquad k \in \mathbb{Z}.$$

Using (27) and assuming $\text{sign}(\delta_1) = \text{sign}(\delta_2)$, that is, that the two trochoids have the same sense, one may obtain analytical solution for the problem:[11]

$$t_A = \frac{t_{2\pi}}{\delta_1 2\pi}\left[\sin^{-1}\left(\frac{\beta}{s_0}\sin(\alpha)\right) + \alpha - \phi_{t_1}\right], \tag{29}$$

where

$$\alpha = \tan^{-1}\left(\frac{y_{t_{20}} - y_{t_{10}}}{x_{t_{20}} - x_{t_{10}} + \beta\frac{\phi_{t_1} - \phi_{t_2} + 2k\pi}{\delta_2\omega}}\right)$$

is the tangent angle defining the direction of the connecting straight segment.

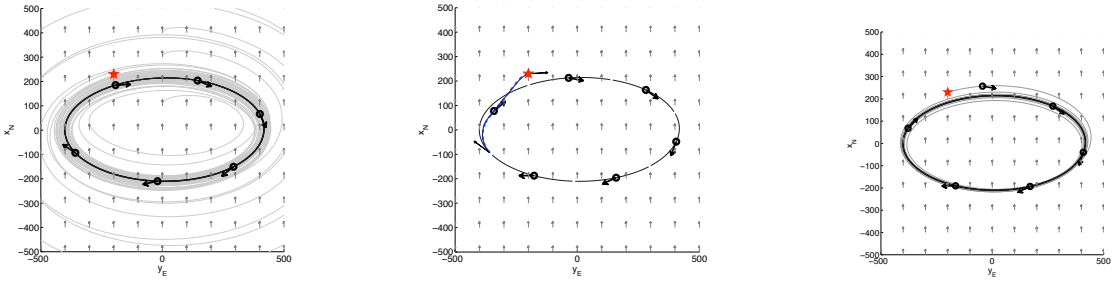

(a) Time-splay coordination. (b) Minimum time alert response. (c) Returning to patrol.

Figure 4. Simulation of coordinated perimeter coverage with time-optimal alert response around a general ellipsoidal curve.

Proposition IV.1.[11] *Define the path* $\gamma(t)$, $t \in [0, T]$, *such that*

$$\gamma(t) = \begin{pmatrix} x_{t_1}(t) \\ y_{t_1}(t) \end{pmatrix} \qquad t \in [0, t_A]$$

$$\gamma(t) = \begin{pmatrix} x_{t_1}(t_A) + \dot{x}_{t_1}(t_A)(t - t_A) \\ y_{t_1}(t_A) + \dot{y}_{t_1}(t_A)(t - t_A) \end{pmatrix} \qquad t \in [t_A, t_\beta]$$

$$\gamma(t) = \begin{pmatrix} x_{t_2}(t - t_\beta + t_B) \\ y_{t_2}(t - t_\beta + t_B) \end{pmatrix} \qquad t \in [t_\beta, T],$$

where

$$t_\beta = t_A + \frac{\sqrt{(x_{t_2}(t_B) - x_{t_1}(t_A))^2 + (y_{t_2}(t_B) - y_{t_1}(t_A))^2}}{\sqrt{\dot{x}_{t_2}(t_B)^2 + \dot{y}_{t_2}(t_B)^2}} \tag{30}$$

$$T = t_\beta + (t_{2\pi} - t_B), \tag{31}$$

and

$$\alpha = \tan^{-1}\left(\frac{y_{t_{20}} - y_{t_{10}}}{x_{t_{20}} - x_{t_{10}} + \beta\frac{\phi_{t_1} - \phi_{t_2} + 2k\pi}{\delta_2 \omega}}\right),$$

$$t_A = \frac{t_{2\pi}}{\delta_1 2\pi}\left[\sin^{-1}\left(\frac{\beta}{s_0}\sin(\alpha)\right) + \alpha - \phi_{t_1}\right],$$

$$t_B = t_A + \frac{\phi_{t_1} - \phi_{t_2} + 2k\pi}{\delta_2 \omega}, \quad k \in \{-3, -2, -1, 0, 1, 2\}.$$

The path $\gamma(t)$ *satisfies the necessary conditions for time-optimality.* □

V. Simulation Results

The proposed framework has been tested in simulations. Two separate cases are considered. In the first case we assume an ellipsoidal base perimeter with semi-major axis $a = 400$m and semi-minor axis $b = 200$m that is to be patrolled by $N = 6$ UAVs. In the second case we select the patrol perimeter of Wright-Patterson Air Force Base (WPAFB). The base perimeter is defined by the convex hull of a finite set of waypoints that were selected at landmarks around WPAFB. The base perimeter was then patrolled by $N = 4$ UAVs.

V.A. Ellipsoidal Base Perimeter

For this case the wind speed was chosen to be $V_w = 5$ m/s from the South, the airspeed of the UAVs was $V_a = 20$ m/s. The initial condition for the UAVs was chosen such that all UAVs were heading North along a straight line ($y_{E_k} = 0, \quad k = 1, ..., N$) when the simulation began. After all UAVs converged to

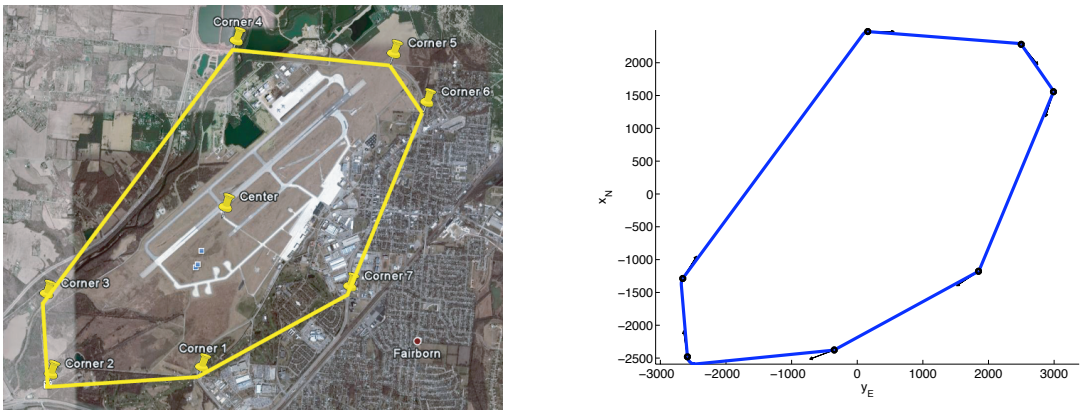

(a) Satellite map of WPAFB.

(b) Strictly convex curve around WPAFB.

Figure 5. Seven points were selected around WPAFB to define a closed convex curve. The curve then serves as the perimeter to be patrolled by a team of UAVs. The straight segments are approximated by arcs of circles of radius $R_0 = 50$km.

the $(M, N) = (6, 6)$ time-splay formation, an intrusion alert was simulated outside of the perimeter (at location $[x_N, y_E]^T = [230\text{m}, -200\text{m}]^T$), see Figure 4(a). After the intrusion was detected, the next UAV in line left the original patrol perimeter to fly to the intrusion point in minimum time (which for the present simulation was $T = 16.9$s), as illustrated in Figure 4(b). While the UAV was following the minimum time path to the intrusion location, the virtual coordinates were shared with the rest of the group to make sure the investigation does not brake the formation. After the prosecutor UAV reached the intruder location, it started the coordination algorithm again (equation (19)) to converge back to the formation (Figure 4(c)).

If the prosecutor UAV had detected the intrusion again, it would have reported it to the rest of the group, and the next UAV in line could then begin to follow the minimum time path to the new intrusion location. If the intruder is not detected again (which was the case in the present simulation), the UAVs resume the coordinated perimeter patrol.

V.B. Wright-Patterson Air Force Base

For this case the wind speed was chosen to be $V_w = 10$ m/s from the South, the airspeed of the UAVs was $V_a = 20$ m/s. Seven points were selected arbitrarily around the "perimeter" of WPAFB. Time-optimal trajectories between the corner-points with the defined initial and final headings were designed using the algorithm described in Section IV.B. The resulting closed path is a convex curve in the plane with maximum rate turns at the curve corners.

The synchronization algorithm (19) requires the curvature to be non-zero everywhere along the closed convex curves. To transform the closed convex path to a strictly convex path with nonzero curvature, the straight segments were approximated with a circle of radius $R_0 = 50$km.[9] Figure 5(a) shows a satellite map of WPAFB with the seven selected GPS coordinates around the base, and Figure 5(b) shows the resulting closed, strictly convex curve in the plane.

In this case the base perimeter was patrolled by $N = 4$ vehicles. Similarly to the previous case, an intrusion alert was simulated after all UAVs have converged to the desired time-phase arrangement, $(M, N) = (4, 4)$. The location of the intrusion point was at $[x_N, y_E]^T = [1300\text{m}, -1250\text{m}]^T$), see Figure 6(a). After the intrusion was detected, the next UAV in line left the original patrol perimeter to fly to the intrusion point in minimum time (which for the present simulation was $T \approx 129$s), as illustrated in Figure 6(b). While the UAV was following the minimum time path to the intrusion location, the virtual coordinates were shared with the rest of the group to make sure the investigation does not disrupt the patrol. After the prosecutor UAV reached the intruder location, it started the coordination algorithm again (equation (19)) to converge back to the formation (Figure 6(c)).

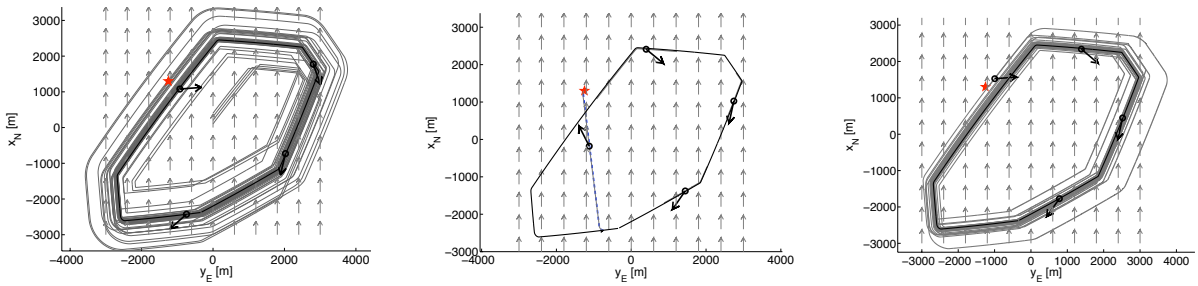

(a) Time-splay coordination. (b) Minimum time alert response. (c) Returning to patrol.

Figure 6. Simulation of coordinated perimeter coverage with time-optimal alert response around WPAFB.

VI. Conclusion

The paper presents a decentralized feedback framework for coordinated base defense with multiple UAVs in steady, uniform wind. Using this framework, a base-defense algorithm is proposed to achieve (1) coordinated motion on convex perimeters; and (2) minimum-time alert response. Theoretical justification for the algorithm is provided. We illustrate the base-defense algorithm using two sets of numerical simulations: first on a simple ellipse boundary and secondly on the boundary of the Wright-Patterson Air Force Base. In ongoing work, we seek to integrate a more detailed model of the intruder spatiotemporal dynamics.

References

[1]Justh, E. W. and Krishnaprasad, P. S., "Equilibria and Steering Laws for Planar Formations," *Systems and Control Letters*, Vol. 52, No. 1, 2004, pp. 25–38.

[2]Frew, E. W., Lawrence, D. A., and Morris, S., "Coordinated Standoff Tracking of Moving Targets Using Lyapunov Guidance Vector Fields," *J. Guidance, Control, and Dynamics*, Vol. 31, No. 2, 2008, pp. 290–306.

[3]Summers, T. H., Akella, M. R., and Mears, M. J., "Coordinated Standoff Tracking of Moving Targets: Control Laws and Information Architectures," *J. Guidance, Control, and Dynamics*, Vol. 32, No. 1, 2009, pp. 56–69.

[4]Sepulchre, R., Paley, D. A., and Leonard, N. E., "Stabilization of planar collective motion: All-to-all communication," *IEEE Trans. Automatic Control*, Vol. 52, No. 5, 2007, pp. 811–824.

[5]Sepulchre, R., Paley, D. A., and Leonard, N. E., "Stabilization of planar collective motion with limited communication," *IEEE Trans. Automatic Control*, Vol. 53, No. 3, 2008, pp. 706–719.

[6]Paley, D. A., Leonard, N. E., and Sepulchre, R., "Stabilization of symmetric formations to motion around convex loops," *Systems and Control Letters*, Vol. 57, No. 3, 2008, pp. 209–215.

[7]Paley, D. A. and Peterson, C., "Stabilization of Collective Motion in a Time-Invariant Flowfield," *J. Guidance, Control, and Dynamics*, Vol. 32, No. 3, 2009, pp. 771–779.

[8]Techy, L., Woolsey, C. A., and Schmale, D. G., "Path Planning for Efficient UAV Coordination in Aerobiological Sampling Missions," *Proc. IEEE Conf. Decision and Control*, Cancun, Mexico, December 2008, pp. 2814–2819.

[9]Techy, L., Paley, D. A., and Woolsey, C. A., "UAV Coordination on Convex Curves in Wind: An Environmental Sampling Application," Accepted to European Control Conference 2009.

[10]Paley, D. A., "Cooperative Control of an Autonomous Sampling Network in an External Flow Field," *Proc. 47th IEEE Conf. Decision and Control*, Cancun, Mexico, December 2008, pp. 3095–3100.

[11]Techy, L. and Woolsey, C. A., "Minimum-Time Path Planning for Unmanned Aerial Vehicles in Steady, Uniform Winds," *Journal of Guidance, Control, and Dynamics*, Accepted, to appear.

[12]Boissonat, J. D., Cerezo, A., and Leblond, J., "Shortest Paths of Bounded Curvature in the Plane," *Proc. of the IEEE International Conference on Robotics and Automation*, Nice, France, May 1992.

[13]McGee, T. G. and Hedrick, J. K., "Optimal Path Planning with a Kinematic Airplane Model," *Journal of Guidance, Control, and Dynamics*, Vol. 30, No. 2, 2007, pp. 629 – 633.

[14]Rysdyk, R. T., "Course and Heading Changes in Significant Wind," *Journal of Guidance Control and Dynamics*, Vol. 30, No. 4, 2007, pp. 1168 – 1171.